



Universiteit  
Leiden  
The Netherlands

## Selectivity and competition between the anodic evolution of oxygen and chlorine

Vos, J.G.

### Citation

Vos, J. G. (2019, December 4). *Selectivity and competition between the anodic evolution of oxygen and chlorine*. Retrieved from <https://hdl.handle.net/1887/81383>

Version: Publisher's Version

License: [Licence agreement concerning inclusion of doctoral thesis in the Institutional Repository of the University of Leiden](#)

Downloaded from: <https://hdl.handle.net/1887/81383>

**Note:** To cite this publication please use the final published version (if applicable).

Cover Page



Universiteit Leiden



The handle <http://hdl.handle.net/1887/81383> holds various files of this Leiden University dissertation.

**Author:** Vos, J.G.

**Title:** Selectivity and competition between the anodic evolution of oxygen and chlorine

**Issue Date:** 2019-12-04

# 7

## MODIFICATION OF SELECTIVITY BETWEEN CHLORINE AND OXYGEN EVOLUTION ON IRIIDIUM-BASED ANODES AND Pt USING SiO<sub>x</sub>-BASED BURIED INTERFACES

In Chapter 6, it was found that a permselective effect versus chloride ions underlies the high OER selectivity of MnO<sub>x</sub>-based anodes, in effect forming a 'buried interface'. This approach would allow selective OER on an otherwise unselective catalyst, and thus seawater electrolysis without chlorine formation. Sadly, there is currently little research in this area, and more overlayer materials capable of preventing chlorine evolution are highly desired. In this chapter, we investigate the effect of thin (5-20 nm) overlayer films composed of amorphous silicon oxide (SiO<sub>x</sub>), which is an electrochemically inert material resistant to acid. We found that the SiO<sub>x</sub> overlayer can be an effective barrier against the CER on flat, relatively well-defined Pt surfaces. On SiO<sub>x</sub>/IrO<sub>x</sub>/GC electrodes, which are more closely related to Ir-based catalysts used in electrolyzers, the CER was not completely suppressed. The CER likely took place at defects in the film, caused by incompatibility of the spin-coating procedure used to produce the films. On the other hand, industrial-type Ir anodes based on Ti, to which significantly thicker films were applied, showed much better CER suppression, although this came at a cost of rather low activity. Although these initial results leave room for improvement, they can further the development of OER- selective anodes.

THIS CHAPTER IS BASED ON THE FOLLOWING

### P U B L I C A T I O N :

Vos, J. G.; Bhardwaj, A.A.; Jeremiase, A.W.; Esposito, D.V; Koper, M. T. M. Modification of Selectivity Between Chlorine and Oxygen Evolution on Iridium-based Anodes and Pt Using SiO<sub>x</sub>-Based Buried Interfaces. Manuscript in preparation (2019).



## 7.1. Introduction

In Chapter 6, we observed that an  $\text{IrO}_x$  electrocatalyst coated by electrodeposited manganese oxide ( $\text{MnO}_x$ ) owes its unusually high OER selectivity in acidic chloride electrolytes to the permselective behavior of the  $\text{MnO}_x$  overlayer, which effectively shielded the catalytically active  $\text{IrO}_x$  from chloride ions. The results of this study are in-line with a recent review that suggests to steer the selectivity between competing reactions by applying a porous, electrochemically inert coating on the catalytic surface.<sup>283</sup> Such coatings can selectively impact the transport between the bulk and the underlying electrochemically active surface. When chosen properly, only the desired reactant can permeate the overlayer, such that a single reaction is promoted on an otherwise unselective catalyst. Besides selectivity, the coating may also improve catalyst stability by providing mechanical support and by shielding the active catalyst from harmful side-reactions, such as the specific attack by chloride on the noble-metal component of iridium-based double perovskites seen in Chapter 3. So-called membrane-coated electrocatalysts (MCEC) therefore hold great potential in solving selectivity problems, as they circumvent the apparent scaling between OER and CER activity. However, MCECs are still in a very early stage of development and have been little investigated. To realize a properly functioning overlayer, the thickness and stability have to be optimal. Ideally, the film is just thick enough to block the undesired reaction, with minimal negative impact on mass transport related to the desired reaction. At the same time, the film must be stable and durable so that its integrity is guaranteed for prolonged times of operation.

Although the  $\text{MnO}_x$ -based overlayer in Chapter 6 was effective at suppressing the CER, it is not expected to be stable for extended periods in acid.<sup>240</sup> Other recent work demonstrates that nanometer-thick silicon oxide ( $\text{SiO}_x$ ) overlayers, which can be spin-coated onto planar Pt surfaces in a well-controlled way, can also form a buried interface.<sup>282</sup> The  $\text{SiO}_x/\text{Pt}$  surfaces were active for the evolution of gaseous hydrogen in presence of  $\text{Cu}^{2+}$ , which normally inhibits the reaction via under-potential deposition. In contrast to  $\text{MnO}_x$ , silicon oxides are expected to be thermodynamically stable in acid and at high potentials.<sup>287</sup> A  $\text{SiO}_x$  overlayer deposited onto known OER/CER catalysts could thus form a promising system for OER-selective seawater electrolysis in neutral or acidic media.

In this chapter, we explore the concept of a buried interface for enhancing selectivity towards the evolution of oxygen instead of chlorine in acidic chloride solutions, by depositing the previously described  $\text{SiO}_x$  overlayer on Pt, thin-layered amorphous iridium oxide ( $\text{IrO}_x$ ), and  $\text{IrO}_2$ -based catalysts on a Ti support (termed Ti-based anodes) as model catalyst surfaces. Of these catalysts, Pt has shown significant capability for CER electrocatalysis, and as it has been studied repeatedly for  $\text{SiO}_x$  deposition, this system forms a convenient reference point.<sup>282,283,288</sup>  $\text{IrO}_x$  and Ti-based anodes are representative for actual anodic materials used in acidic and near-neutral water electrolysis.<sup>152,171,289</sup> Thin-layered  $\text{IrO}_x$  nanoparticles would be a relatively well-defined model system for Ir-based electrocatalysts and were included for this reason. Ti-based anodes were prepared by Magneto Special Anodes (an Evoqua brand) according to a procedure identical to that for large-scale, commercial anodes.<sup>33</sup> Results

obtained from the study of these materials could in principle be directly translated to industrial conditions.

## 7.2. Experimental

### 7.2.1. *Electrochemical procedures*

KHSO<sub>4</sub> and KCl (EMSURE) were purchased from Merck and used as received. The water used for all experiments was prepared by a Merck Millipore Milli-Q system (resistivity 18.2 MΩcm, TOC < 5 p.p.b.).

All experiments were carried out at room temperature (~20 °C). The electrochemical experiments were done using home-made two-compartment borosilicate glass cells with solution volumes of 100 mL. Before first-time use, all glassware was thoroughly cleaned by boiling in a 3:1 mixture of concentrated H<sub>2</sub>SO<sub>4</sub> and HNO<sub>3</sub>. When not in use, all glassware was stored in a 0.5 M H<sub>2</sub>SO<sub>4</sub> solution containing 1 g/L KMnO<sub>4</sub>. Before each experiment, glassware was thoroughly rinsed with water, and then submerged in a dilute (~0.01 M) solution of H<sub>2</sub>SO<sub>4</sub> and H<sub>2</sub>O<sub>2</sub> to remove all traces of KMnO<sub>4</sub> and MnO<sub>2</sub>. The glassware was then rinsed three times with water and boiled in water. The rinsing-boiling procedure was repeated two more times.

An IviumStat potentiostat (Ivium Technologies) with the IviumSoft package was used during electrochemistry experiments. All experiments involving electrocatalytic chlorine and oxygen evolution were 95% iR-compensated. The solution resistance was measured with electrochemical impedance spectroscopy, by observing the absolute impedance in the high frequency domain (100-10 KHz) corresponding to a zero-degree phase angle. Working solutions of 0.5 M KHSO<sub>4</sub> were saturated with Ar (Linde, purity 6.0) before experiments. Solutions were bubbled with Ar gas during forced convection experiments, Ar was used to blanket the solution in case of stationary conditions. The reference electrode for all RRDE experiments was a HydroFlex® reversible hydrogen electrode (Gaskatel), separated from the main solution using a Luggin capillary, to fix the reference sensing point and to prevent mixed potentials at the reference due to dissolved Cl<sub>2</sub> gas. All potentials in this chapter are reported versus the RHE scale. The counter electrode was a Pt mesh, separated from the main solution by a coarse glass frit.

RRDE measurements were done with a MSR rotator and E6 ChangeDisk RRDE tips in a PEEK shroud (Pine Research). The Luggin tip connected to the reference electrode was aligned to the center of the RRDE electrode to minimize electrical cross-talk.<sup>137,138</sup> Before chlorine or oxygen collection experiments, the Pt ring was electropolished by scanning from -0.1 V to 1.7 V at 500 mV s<sup>-1</sup> for 40 scans at 1500 RPM. The ring was kept at 0.95 V to selectively probe the CER in parallel with the OER, and at 0.40 V to probe the evolution of O<sub>2</sub> in chloride-free electrolytes. Ring currents were corrected for constant background currents and product collection delay, the latter arises from the time needed for products formed on the disk to reach the ring.<sup>290</sup>

## 7.2.2. Electrode preparation

### 7.2.2.1. $\text{IrO}_x/\text{GC}$

Commercial GC RDE disk inserts of 5 mm diameter were purchased from Pine Research. After hand-polishing the surface with diamond suspension and sonication in water, a thin  $\text{IrO}_x$  layer was electroflocculated onto the GC surface from a hydrated  $\text{IrO}_x$  colloid solution at acidic pH. Full details can be found in section 9.1.

### 7.2.2.2. $\text{Pt}/\text{Ti}/\text{GC}$

Commercial GC RDE disk inserts of 5 mm diameter were purchased from Pine Research. A 2 nm layer of Ti (99.99%) and 3 nm layer of Pt (99.99%) were sequentially deposited onto the GC surface at  $0.2 \text{ A s}^{-1}$  by electron-beam evaporation without breaking vacuum and without substrate heating in a Angstrom EvoVac evaporator system, with a base pressure of  $1.0 \times 10^{-7}$  Torr. A commercial Pt disk from Pine Research served as  $\text{SiO}_x$ -free reference material.

### 7.2.2.3. *Ti-based anodes*

Commercial Ti (grade 2) RDE disk inserts of 5 mm diameter were purchased from Pine Research. Two types of  $\text{IrO}_2$ -based catalysts, a mixture of  $\text{IrO}_2$  and  $\text{Ta}_2\text{O}_5$  and one of  $\text{IrO}_2$  and Pt, were prepared on these electrodes by Magneto Special Anodes (an Evoqua brand), using a thermal decomposition method.

### 7.2.2.4. $\text{SiO}_x$ deposition

Trimethylsiloxy-terminated polydimethylsiloxane (PDMS) dissolved in toluene was spin-coated onto the fixated disk samples with an acceleration to a speed of 2400 rpm over 3 seconds, followed by a ramp to 4000 rpm over 30 seconds and maintained speed at 4000 rpm for 2 minutes following. The solvent was then evaporated by drying the electrodes in a vacuum oven at  $90 \text{ }^\circ\text{C}$  for 60 min. To obtain  $\text{SiO}_x$ , the final PDMS coating was chemically oxidized in a UV-ozone cleansing chamber for 2 h (UVOCS, T10X10/OES). The eventual  $\text{SiO}_x$  film thicknesses were varied by changing the concentration of PDMS in the toluene solutions, and repeating the spin-coating and drying procedure as necessary. For the  $\text{SiO}_x/\text{Pt}/\text{Ti}/\text{GC}$  samples with film thicknesses of 5 nm  $\text{SiO}_x$ , a single spin-coating step using a 5.3 mg/L solution of PDMS in toluene was chosen. Four  $\text{SiO}_x/\text{IrO}_x/\text{GC}$  samples were made with varied procedures to fabricate the  $\text{SiO}_x$  overlayer. For sample 1, one drop of 10 mg/mL PDMS in toluene was used. For samples 2 and 3, two complete fabrication cycles were performed on each sample using one drop of 10 mg/mL PDMS in toluene for spin-coating, and for sample 4, two complete fabrication cycles were performed using two drops of 10 mg/mL PDMS in toluene. The targeted  $\text{SiO}_x$  overlayer thicknesses for these three procedures were 5 nm, 10 nm, and 20 nm, respectively. For the Ti-based anodes, 3 complete fabrication cycles were performed using 50 mg/L PDMS in toluene for spin-coating. The targeted  $\text{SiO}_x$  thickness on the Ti-based anodes was 10 nm. We note that the thickness of the overlayer may vary over the relatively rough surface of the Ir-based electrodes, especially regarding the industrial ones with Ti supports.

The thickness values for the Ir-based samples are provided as very rough estimates and not measured values.

### 7.2.3. Voltammetry procedures during electrocatalysis

All currents were reported as densities per geometrical surface area. Normalization to the ‘real’ catalyst surface area, which is an inherently difficult topic in electrocatalysis research (see section 3.3.2), was not pursued. In this chapter we were only interested in ratios of currents, namely selectivity values and comparisons of activity before and after applying a SiO<sub>x</sub> overlayer. The electron beam-deposited Pt surfaces have a very low roughness (<1 nm), such that their active surface area is approximately equal to the geometrical one.<sup>282</sup>

#### *7.2.3.1. Pt*

All Pt electrodes were pre-treated before scanning by conditioning at 0.40 V and 0.70 V for 10 s and 3 s, respectively (see Figure A 9.7.1), while rotating. This was done to ensure that the surfaces were oxide-free and reproducible. Linear potential sweeps were performed immediately after on the Pt-based electrodes between 0.70 – 1.90 V, at 10, 20 and 50 mV s<sup>-1</sup>, under varying rotation rates. In-between experiments, the electrodes were kept at 0.05 V.

#### *7.2.3.2. IrO<sub>x</sub> and Ti-based anodes*

Before initiating quantitative measurements, all Ir-based electrodes were scanned 20 times in a chloride-free electrolyte between 1.3 – 1.55 V (into the OER region) at 1500 RPM. This was done to ensure stable behavior during experiments by equilibrating the Ir-centers (see below). Similar to Pt, a two-step potential-holding program preceded every catalytic cycle. The IrO<sub>x</sub> surfaces were conditioned for 10 s and 3 s at 0 V and 1.3 V, respectively; for the IrO<sub>2</sub> + Ta<sub>2</sub>O<sub>5</sub> catalyst, the procedure was 10 s and 5 s at 0 V and 1.3 V, and for IrO<sub>2</sub> + Pt, it was 10 s and 6 s at 0.05 V and 1.3 V (see also Figure A 9.7.1). After the pretreatment, all Ir-based catalysts were probed for OER and CER electrocatalysis between 1.3 – 1.55 V at 10 mV s<sup>-1</sup> and 1500 RPM.

### 7.2.4. Scanning electron microscopy (SEM) and energy-dispersive X-ray spectroscopy (EDS)

RDE inserts were carefully removed from the RRDE tip after electrochemical experiments and glued to a SEM specimen mount using conductive silver paint. The silver paint was dried for 3 hours in air under reduced pressure. SEM micrographs were obtained using an Apreo S SEM setup (Thermo Scientific) equipped with a field emission electron source and EDS detector. Images were recorded in immersion mode using a through-the-lens detector, at a working distance of ~4.0 mm, with 10 kV beam acceleration voltage and a beam current of 0.4 pA. EDS measurements were performed at the same beam voltage and current.

## **7.3. Results and discussion**

In the following, RRDE voltammetry will be used to probe the kinetics and selectivity of the OER and CER on a variety of SiO<sub>x</sub>-modified catalysts. Use of an RRDE ensures well-defined mass transport conditions, which is important concerning accurate statements of selectivity

where one reaction is fast and strongly dependent on diffusion. The use of interchangeable electrodes may cause some damage to the  $\text{SiO}_x$  overlayer films, as will be described below. Nonetheless, the method was chosen as it offers the highly attractive option to separate the OER and CER current densities as described in Chapter 2. Capacitive scanning contributions to the disk current were minimized by using relatively slow scan rates, and averaging the values from forward and backward scans for Ir-related experiments. For the Pt experiments, a constant value was subtracted from the linear sweep voltammograms based on pseudo-capacitive charging seen around the onset of platinum oxide formation.

### 7.3.1. Pt

As described in the introduction, the  $\text{SiO}_x/\text{Pt}$  electrode is a convenient reference point for looking closely at parallel OER and CER and the effect of the  $\text{SiO}_x$  overlayer. It must be noted that pure Pt is not popular for actual electrolyzers, due to its high price and rather poor OER performance.<sup>83</sup> At high potentials the catalytic activity is also impacted by the formation of platinum oxides ( $\text{PtO}_x$ ), which will be discussed below.

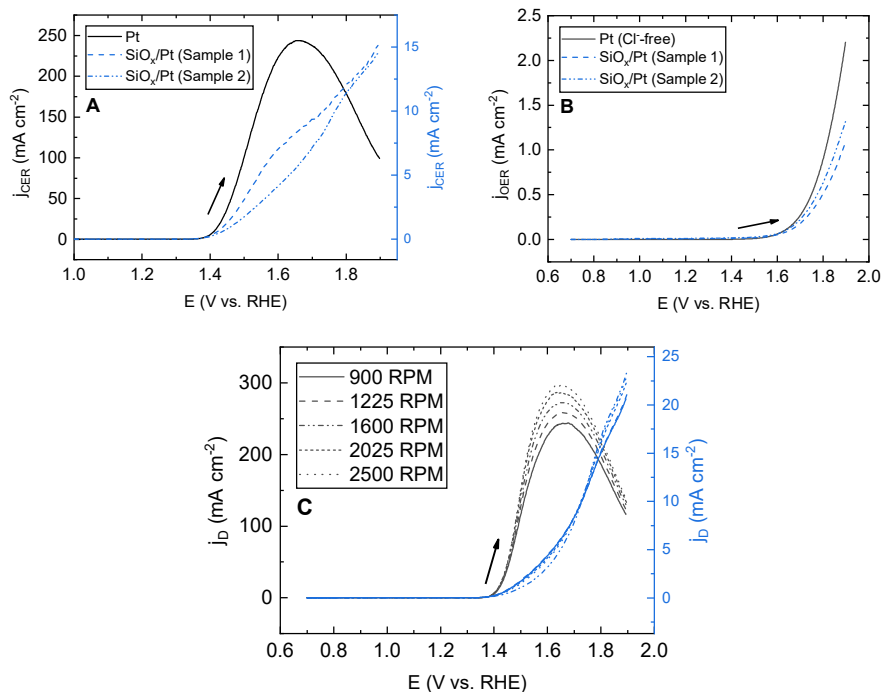


Figure 7.1: Effect of a  $\text{SiO}_x$  overlayer on the electrocatalytic behavior of Pt in acidic chloride-containing media. A: Current densities of the CER on a Pt disk electrode (black) and two  $\text{SiO}_x/\text{Pt}/\text{Ti}/\text{GC}$  electrodes with a 5 nm  $\text{SiO}_x$  overlayer (blue), in  $0.5 \text{ M KHSO}_4 + 0.6 \text{ M KCl}$ . Note the difference in scale.  $j_{\text{CER}}$  was derived from ring currents as described in Eq. 2.3. Rotation rate 1600 RPM, LSVs recorded at  $10 \text{ mV s}^{-1}$ . B: 'Pure' OER activity on Pt (black) and on the  $\text{SiO}_x$ -coated Pt samples (blue), in  $0.5 \text{ M KHSO}_4$  (chloride-free conditions). C: Measured disk current density versus rotation rate on Pt (black) compared to a 5 nm  $\text{SiO}_x/\text{Pt}/\text{GC}$  electrode (blue), in  $0.6 \text{ M chloride}$ , recorded at  $20 \text{ mV s}^{-1}$ . Arrows indicate scan direction.

Figure 7.1 shows some typical results of parallel OER and CER on Pt surfaces both ‘free’ and covered by a SiO<sub>x</sub> overlayer. The CER activity data were measured in presence of 0.6 M KCl, which corresponds to the average chloride concentration of natural seawater.<sup>291</sup> On an unmodified Pt electrode (black trace in Figure 7.1A), chlorine evolution has a clear onset around 1.37 V, after which the rate goes through a maximum and declines. The latter can be ascribed to inhibiting effects from PtO<sub>x</sub> formation at high potentials.<sup>292</sup> It has been previously reported that PtO<sub>x</sub> already interferes with the CER around its onset.<sup>58,118,293</sup> The peak CER current seen in Figure 7.1A is around 16% of the value predicted by the Levich equation, meaning that the maximum is significantly lower than would be expected from diffusion-limitations. In presence of a SiO<sub>x</sub> overlayer (blue traces), the CER activity is strongly inhibited and decreases roughly 20-fold. The OER activity (measured in absence of chloride) in Figure 7.1B is only moderately impacted by the overlayer. It was verified that the OER still occurs on the SiO<sub>x</sub>-encapsulated catalyst by using the RRDE with the Pt ring fixed at 0.4 V in chloride-free conditions, showing that O<sub>2</sub> can traverse the overlayer to be detected on the ring (Figure A 9.7.4). The rotation rate dependence of the disk current density is shown in Figure 7.1C. Contrary to bare Pt, there is very little dependence of disk current on the chloride mass transport to the SiO<sub>x</sub>/Pt surface, suggesting that the observed potential-current response (which is largely from chlorine evolution) is dominated by chloride transport through the SiO<sub>x</sub> overlayer.

It is noted that the CER rates on SiO<sub>x</sub>/Pt/Ti/GC in Figure 7.1A no longer show a maximum, which suggests that the overlayer changes how PtO<sub>x</sub> forms during the scan. The voltammetric characterizations in Figure A 9.7.2 illustrate that in presence of the SiO<sub>x</sub> overlayer, the onset of PtO<sub>x</sub> formation is shifted to a higher potential, but more oxide appears to be formed relative to the SiO<sub>x</sub>-free sample, after normalizing the oxide reduction peaks to the electrochemical surface area using the hydrogen desorption region (Figure A 9.7.3). SEM micrographs (Figure A 9.7.15) suggest that the electrode surface is homogeneously covered by SiO<sub>x</sub>. Neither Si associated with the SiO<sub>x</sub> overlayer or Pt and Ti from the electrode and adhesion layer could be identified in EDS analysis due to the limited interaction between the electron beam and these ultrathin layers.

Even though the suppressive effect of SiO<sub>x</sub> on the CER is large, it is not quite as large as measured during a similar study by us using stationary, ideally flat electrodes, where the residual CER activity was close to 0.<sup>294</sup> The samples used in that study had a much larger surface area compared to the RDE disk inserts, which means the fluid dynamics during spin-coating on the disk inserts were non-ideal near the edges. The CER activity in Figure 7.1 may originate from such imperfections since we could not find widespread defects in the overlayer while surveying the surfaces with SEM. Additionally, the disk extremities are unavoidably exposed to force when the disk electrode is inserted into the RRDE assembly. The absence of rotation rate dependence in Figure 7.1C suggests that chloride diffusion relating to the CER activity is still somehow hindered.

The variation of the OER and CER activity as function of the chloride concentration on a SiO<sub>x</sub>/Pt/Ti/GC sample is shown in Figure 7.2. We found that the CER rate on the bare Pt surface (Figure A 9.7.11) displays an approximately linear response to the concentration,

indicating that the chloride reaction order is close to 1, which was found in Chapter 4 as well. In Figure 7.2 however, the  $\text{SiO}_x$ -treated samples have different, more complex concentration dependencies. The top panel of Figure 7.2 shows that the OER activity at the buried interface is slightly suppressed by the addition of chloride, but otherwise not strongly dependent on the chloride concentration.

On bare Pt, the derivation of OER currents in parallel with the CER was unfortunately not possible, due to the high rates of chlorine evolution on such surfaces. These high rates led to macroscopic gas bubbles that lodged at the interspace between the disk and the ring and led to severe distortion of the ring response (see also Chapter 8). The CER currents on the  $\text{SiO}_x/\text{Pt}/\text{Ti}/\text{GC}$  electrodes were much lower, so that it was still possible to use the ring-disk approach in highly concentrated chloride solutions, although the ring response was still slightly erratic; the apparent value of  $N_{\text{Cl}_2}$  varied somewhat ( $\pm 10\%$ ) depending on the sample. This is possibly a result of hindered transport of  $\text{Cl}_2$  across the  $\text{SiO}_x$  film, and leads to the

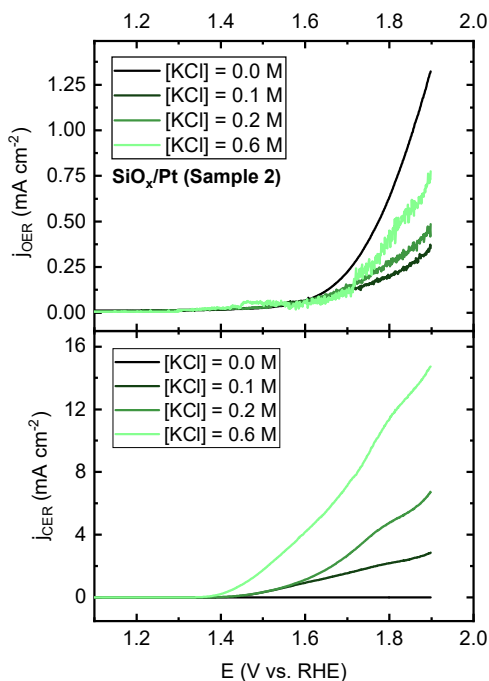


Figure 7.2: Current densities for the OER (top) and CER (bottom) as function of chloride concentration, on a  $\text{SiO}_x/\text{Pt}/\text{Ti}/\text{GC}$  electrode, in  $0.5 \text{ M KHSO}_4$ . Rotation rate  $1600 \text{ RPM}$ , LSVs recorded at  $10 \text{ mV s}^{-1}$ .

somewhat erratic behavior of derived OER currents seen in the top panel of Figure 7.2. To minimize this source of error,  $N_{\text{Cl}_2}$  was calibrated for each experiment by comparing the disk current to the ring response while evolving chlorine in the potential region  $1.50 - 1.55 \text{ V}$ , where the CER is the sole measurable reaction.

Regarding the selectivity between the OER and CER, the precise effect of the SiO<sub>x</sub> overlayer on Pt is not straightforward to summarize, since multiple effects are involved. On the one hand, the overlayer strongly inhibits the CER. On the other hand, it also seems to delay PtO<sub>x</sub> formation, which can favor it. The SiO<sub>x</sub> overlayer also leads to some inhibition of the OER activity when comparing with the free Pt surface (Figure 7.1B), which further increases  $\varepsilon_{CER}$ . Full selectivity data is shown in Figure A 9.7.5. These data, as well as the rest of the selectivity data in this chapter, were derived using Eq. 2.3. One can observe that the free Pt surface shows a significant enhancement of the OER selectivity at high potentials, due to the strong suppression of the CER by oxides. Nonetheless, the most important finding is that the SiO<sub>x</sub> overlayer on Pt greatly impairs the CER, while still allowing the OER to occur.

### 7.3.2. IrO<sub>x</sub>

SiO<sub>x</sub> was deposited onto IrO<sub>x</sub> and it was tested whether the CER could be selectively suppressed. The targeted SiO<sub>x</sub> thickness was 5-20 nm, generally higher than that used for the Pt samples, as even though the IrO<sub>x</sub> layer can be made reasonably flat, we previously found (Chapter 6 and Figure A 9.7.18) that it still has roughness features in the order of 10-100 nm. Four SiO<sub>x</sub>/IrO<sub>x</sub> samples were investigated, together with a SiO<sub>x</sub>-free sample for comparison.

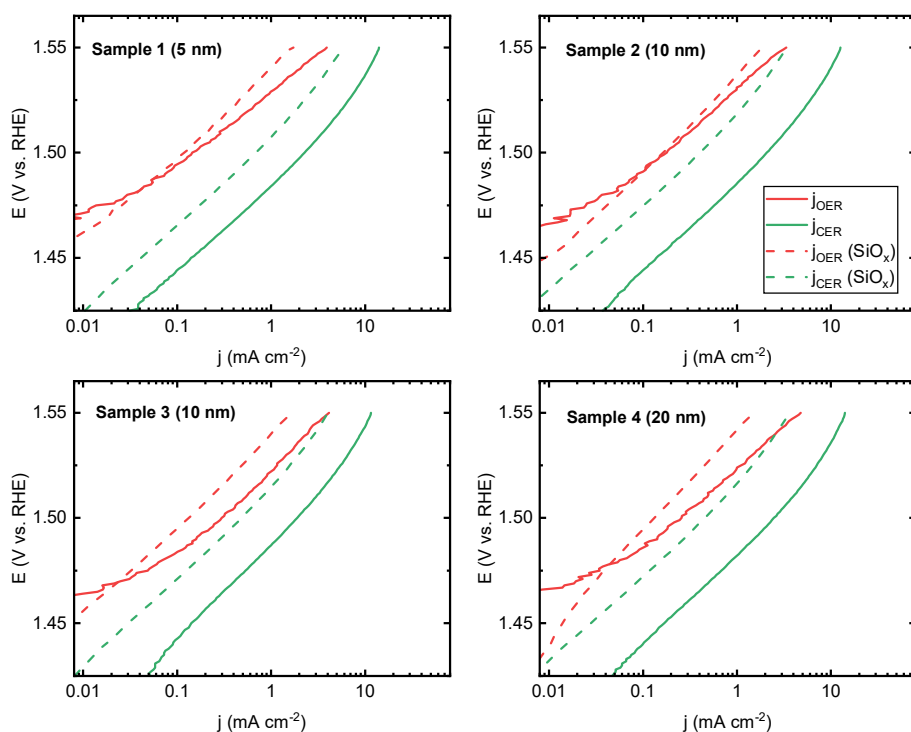


Figure 7.3: Tafel plots for parallel OER and CER on SiO<sub>x</sub>/IrO<sub>x</sub> samples of varying SiO<sub>x</sub> overlayer thicknesses, before and after SiO<sub>x</sub> deposition, in 0.5 M KHSO<sub>4</sub> + 30 mM KCl. Rotation rate 1500 RPM.

Figure 7.3 shows a comparison of Tafel curves of the OER and CER, derived using Eq. 2.3, in a chloride concentration of 30 mM as test case for comparing the sample activities before and after  $\text{SiO}_x$  deposition. The first trace of evolved oxygen appeared between 1.45-1.46 V on these samples, regardless of whether  $\text{SiO}_x$  was present (Figure A 9.7.7). In the presence of a spin-coated  $\text{SiO}_x$  layer, the electrocatalytic activity of the  $\text{IrO}_x$  samples moderately decreases. The Tafel lines of the OER and CER were both shifted to higher potentials. This lowering of activity is usually more severe for the CER, but all  $\text{IrO}_x$  samples still showed considerable CER activity after the  $\text{SiO}_x$  coating. This is contrary to the results for Pt described in section 7.3.1, where the  $\text{SiO}_x$  overlayer on Pt decreased the CER activity to less than a few % relative to the uncoated Pt reference sample. This means that either the  $\text{IrO}_x$  is incompletely covered by the films, or that the films are somehow not as effective with  $\text{IrO}_x$  as the underlayer, in the sense that they could still be permeable to chloride.

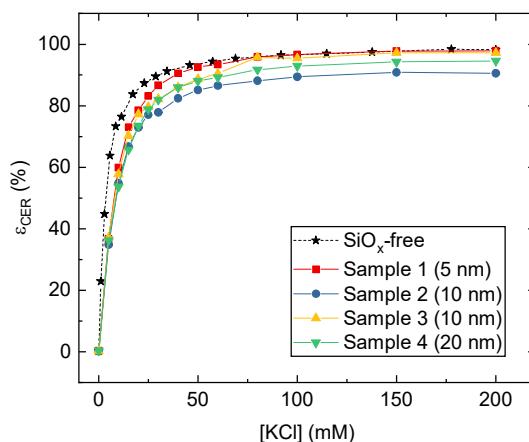


Figure 7.4: Molar selectivity towards the CER as function of chloride concentration for several  $\text{SiO}_x/\text{IrO}_x/\text{GC}$  samples. Values of  $\epsilon_{\text{CER}}$  calculated according to Eq. 2.3. Rotation rate 1500 RPM.

The CER selectivity ( $\epsilon_{\text{CER}}$ ) of the  $\text{SiO}_x/\text{IrO}_x/\text{GC}$  electrodes was measured as a function of chloride concentration, where the upper limit of 200 mM KCl is reasonably close to the actual chloride concentration in seawater (Figure 7.4). Although the samples all show some reduction in CER selectivity compared to the  $\text{SiO}_x$ -free reference sample, there is no clear correlation between the selectivity and the formal  $\text{SiO}_x$  thickness.

In order to look more closely into the effect of the  $\text{SiO}_x$  overlayer, we focused on the kinetics of both reactions, particularly by looking at experimental Tafel slopes and chloride reaction orders  $\mathcal{R}_{\text{Cl}^-}$  (Figure A 9.7.12 and Figure A 9.7.14). Although caution is advised when trying to directly interpret either of these quantities in relation to the ‘true’ underlying reaction mechanism, it is expected that they change significantly when the  $\text{SiO}_x$  overlayer exerts an influence, especially so for the CER. If mass transport is the limiting step, values of  $\mathcal{R}_{\text{Cl}^-}$  for the CER should be 1 and the Tafel slope should approach infinity. These values should be attained as the potential-dependent CER rate exceeds the rate of mass transport. When comparing  $\mathcal{R}_{\text{Cl}^-}$  on the bare  $\text{IrO}_x/\text{GC}$  sample and  $\text{SiO}_x/\text{IrO}_x/\text{GC}$  (section 2 of the supporting

information), there is no obvious change in the values as function of potential. It needs to be noted that CER Tafel curves on all SiO<sub>x</sub>-coated samples have slightly higher slopes around the high potential limit of 1.54 V. They are 65-70 mV/dec, compared to ~55 mV/dec in the reference. This could suggest that the chloride mass transport is decreased by the overlayer, but only to a minor extent. As the OER activity is also slightly suppressed, an additional investigation was performed on the voltammetric characterizations of the samples before and after SiO<sub>x</sub> deposition (Figure A 9.7.6). The presence of SiO<sub>x</sub> seems to suppress the semi-reversible peak observed around 0.94 V, which is ascribed to a redox transition between Ir<sup>3+</sup> and Ir<sup>4+</sup>.<sup>168,250,295</sup> Suppression of the peak shows that the overlayer affects the redox states in the IrO<sub>x</sub> film, and that the overall reaction kinetics could change because the catalytic behavior of IrO<sub>x</sub> intimately depends on the redox state of the Ir centres.<sup>154,296,297</sup> However, we found

(section 2 of the supporting information) that linear Tafel slopes of the OER in all samples ranged between 40-50 mV/dec, and that likewise, the OER activity was little affected by chloride (Figure A 9.7.13), irrespective of the presence of the SiO<sub>x</sub> overlayer. Both observations indicate that the OER mechanism remains the same after applying the SiO<sub>x</sub> coating. Therefore, the SiO<sub>x</sub> likely does not affect the reactivity of the IrO<sub>x</sub> underlayer. Additionally, the significant CER electrocatalysis that occurs on the SiO<sub>x</sub>/IrO<sub>x</sub> samples behaves kinetically the same as on the IrO<sub>x</sub> reference. It is thus probable that the SiO<sub>x</sub> overlayer is incomplete, or locally delaminates during gas evolution.

The surfaces of the samples were explored using SEM, coupled to EDS analysis; Figure A 9.7.16 shows a typical EDS spectrum. Besides Si, Ir and O, large amounts of C were consistently detected due to the bulk GC electrode support. Cl was usually seen as well in low amounts, along with K and S, which correspond to traces of trapped electrolyte. Part of the Cl fraction is likely bound to Ir as a result of incomplete hydrolysis of the chloroiridate precursor (see Chapter 6).

An example micrograph of a SiO<sub>x</sub>/IrO<sub>x</sub>/GC surface is shown in Figure 7.5, together with corresponding elemental maps of Si and Ir (see section 3 of the supporting information for additional micrographs). In Figure 7.5, the SiO<sub>x</sub>-encapsulated IrO<sub>x</sub> is visible as a relatively flat layer with fluffy morphology. EDS analysis shows that the SiO<sub>x</sub> overlayer is present across the entire image. Dark grey areas and Si EDS mapping in Figure 7.5 suggest that the overlayer is not evenly distributed over the surface. Multiple SiO<sub>x</sub> layers are visible that appear folded onto themselves. Si was found globally across the electrode surface, including areas where the IrO<sub>x</sub> layer was interrupted or where local clusters of IrO<sub>x</sub> nanoparticles were formed (Figure A 9.7.20 and Figure A 9.7.21). Zoomed-in micrographs in Figure A 9.7.18 illustrate the morphology of these clusters. Rugged surface structures are difficult to cover properly via spin coating, so that the SiO<sub>x</sub> layer around these clusters could be defective on the nano-scale. It is not possible to register such imperfections with EDS, which is inherently limited to resolutions of around a micrometer. Nonetheless, no indications were found that large areas of the electrode were completely uncovered by SiO<sub>x</sub>. The previously discussed CER activity then probably originates from a select few areas where the electrocatalytic activity is high and the Si overlayer is imperfect, or damaged by local instances of vigorous gas evolution at the buried interface (see Figure A 9.7.22 and Figure A 9.7.23). These results suggest that the adhesion of

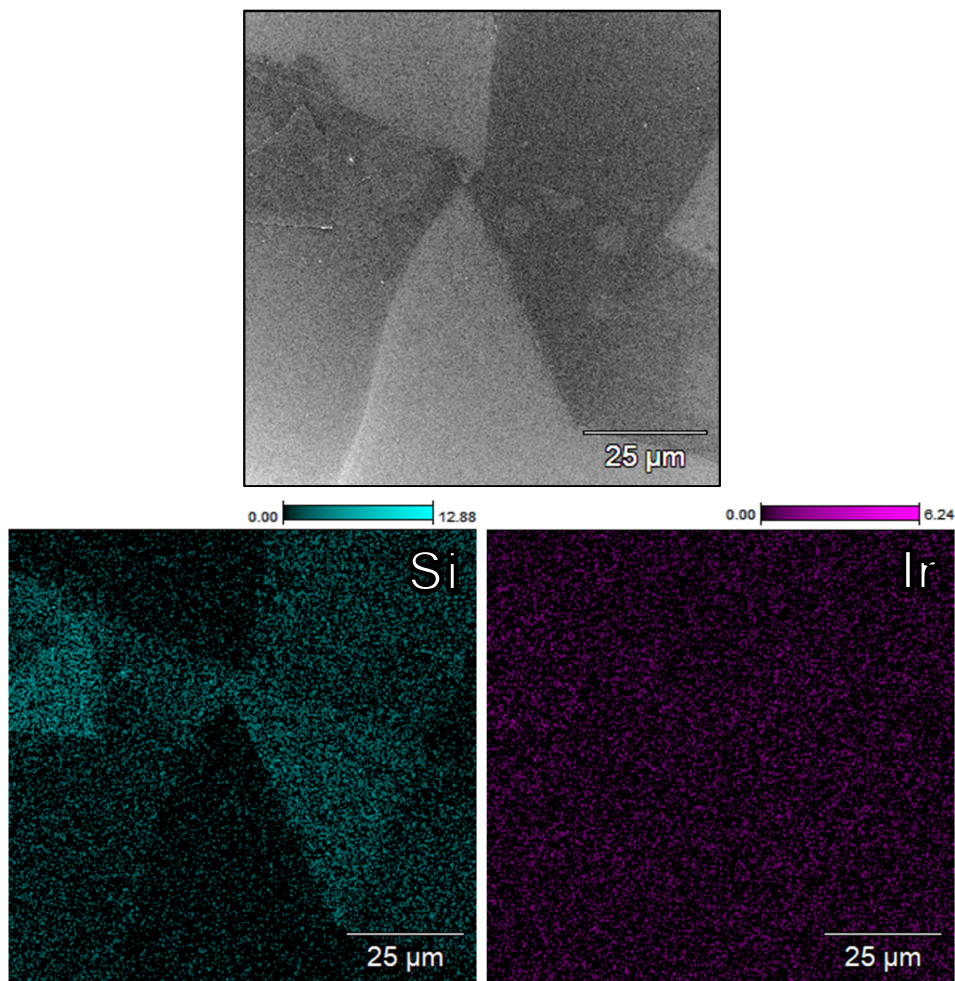


Figure 7.5: SEM micrograph and EDS analysis of a  $\text{SiO}_x/\text{IrO}_x/\text{GC}$  electrode surface, after extensive OER + CER electrocatalysis under forced convection conditions. In the electron image (greyscale), folded sheets of  $\text{SiO}_x$  are visible on top of the  $\text{IrO}_x$  layer. Color images show corresponding elemental mapping of Si and Ir. Scale bars show the amounts of the elements, as atomic percentage of total (which included O and C from the GC substrate, see Figure A 9.7.17).

a desired overlayer may differ substantially, depending on the underlayer, and that care must be taken when translating a functional overlayer design to a different catalyst.

### 7.3.3. Ti-based anodes

The Ti-based anodes are thick layers of metal oxides deposited on Ti disks, with the same method used for large surface area industrial anodes that are sold commercially by Magneto Special Anodes (an Evoqua brand). We tested a sample consisting of a Ti substrate coated by a mixture of  $\text{IrO}_2$  and  $\text{Ta}_2\text{O}_5$  (termed IrTa/Ti), as well as two samples of an  $\text{IrO}_2$  anode containing Pt (termed IrPt/Ti). The samples were probed for OER and CER activity before and

after SiO<sub>x</sub> deposition. As this type of electrode commonly has micrometer-sized roughnesses,<sup>87,298,299</sup> a large amount of SiO<sub>x</sub> precursor was used during deposition to achieve an extra thick overlayer, so that the electrodes were properly encapsulated.

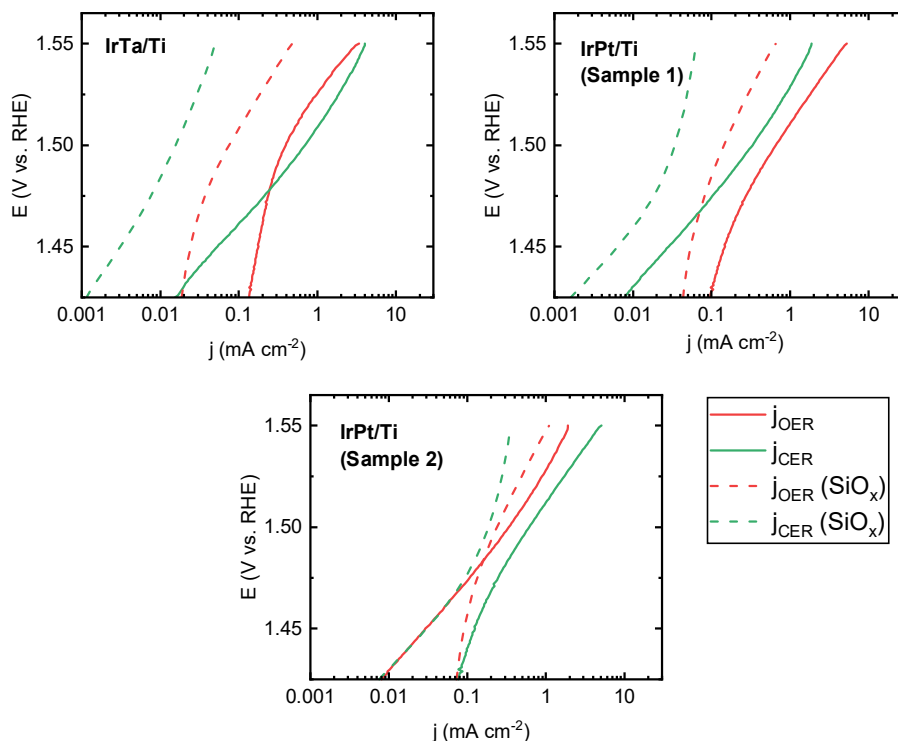


Figure 7.6: Tafel plots for parallel OER and CER on Ti-based anodes, before and after SiO<sub>x</sub> deposition, in 0.5 M KHSO<sub>4</sub> + 30 mM KCl. Rotation rate 1600 RPM.

Like Figure 7.3, Figure 7.6 shows Tafel curves of the Ti-based anode samples in 30 mM KCl, before and after depositing SiO<sub>x</sub>. In these results, there is a significant reduction in overall activity. This activity is roughly an order of magnitude, much more so than for IrO<sub>x</sub>. This is most likely caused by the relatively thick overlayer, which may quickly stifle mass transport as its thickness increases.<sup>283</sup> Evidence for this is visible in the voltammetric characterizations of the samples, which show less features after the coating (Figure A 9.7.8). Besides lower activity, there is also significant suppression of the CER in favor of the OER, which is a favorable finding. The effect is much stronger than seen on IrO<sub>x</sub> in section 7.3.2. In addition to the thicker SiO<sub>x</sub> overlayer, a difference in catalyst morphology may explain the apparently more pronounced selectivity shift on these electrodes, in the sense that the adhesion of the overlayer to the catalyst could become more favorable.

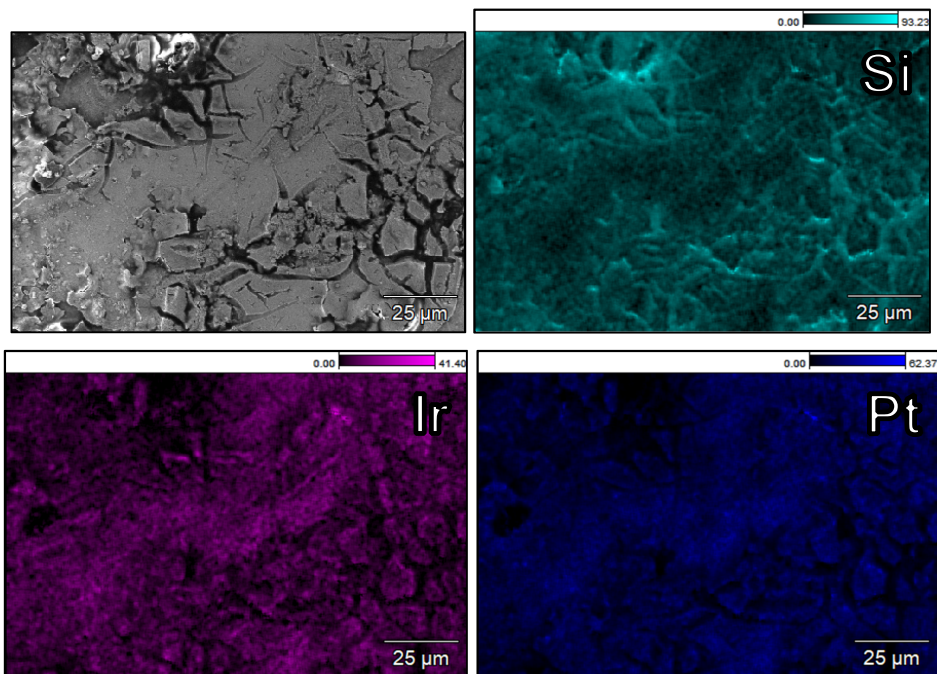


Figure 7.7: SEM micrograph and EDS mapping of an IrPt/Ti electrode surface, after extensive OER + CER experiments under rotation. The electron image is shown in grayscale, colored images show elemental mapping of Si, Ir and Pt. Scale bars show the relative amounts of the elements, as atomic percentage of total (which included Ti, data shown in Figure A 9.7.24).

SEM/EDS analysis of a IrPt sample in Figure 7.7 shows that Si has accumulated in the micrometer-sized cracks of the mixed metal oxides. This accumulation must have occurred

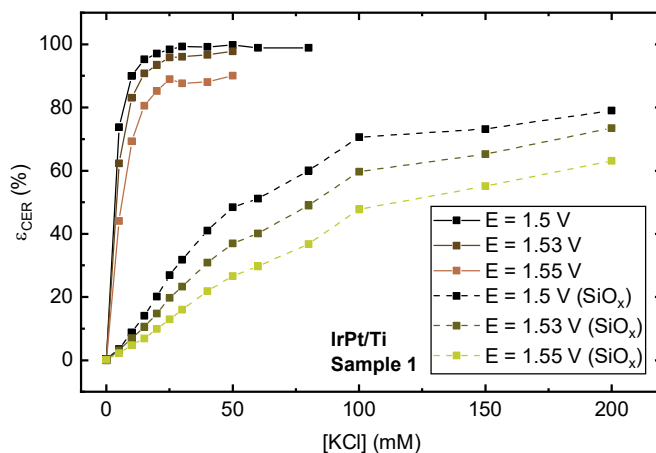


Figure 7.8: Molar selectivity towards the CER as function of chloride concentration for an IrPt/Ti sample, as in Figure 7.4. Values obtained on the original anode (solid, brown lines) are compared to those in presence of the SiO<sub>x</sub> overlayer (beige, dotted lines). Rotation rate 1500 RPM.

during the spin-coating phase, where the PDMS solution infiltrated the catalyst cracks. As the distribution of Si around the cracks is not strongly coupled to carbon (see Figure A 9.7.24), it is probably present as the oxide and not its PDMS precursor. It suggests that despite being isolated within the cracks, the excess PDMS was still successfully oxidized during the plasma treatment, or oxidized later during polarization experiments.

We measured values of  $\epsilon_{CER}$  as function of chloride concentration for the mixed metal oxides, as was done for the IrO<sub>x</sub> samples. The effect of the SiO<sub>x</sub> overlayer on the CER selectivity, as shown in Figure 7.8, is obvious. The OER is significantly more favored, especially at low (<30 mM) KCl concentrations. A similar trend was seen on the other Ti-based anode samples, although the effect is not perfectly reproducible among samples (see Figure A 9.7.9 and Figure A 9.7.10). This is likely due to the inhomogeneity of the surfaces.

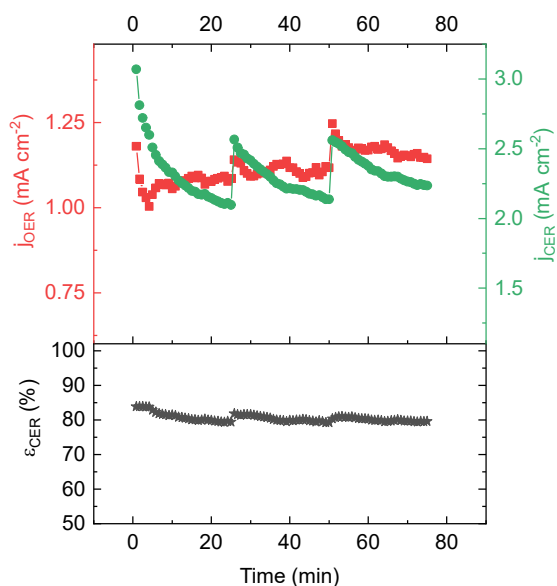


Figure 7.9: Accelerated lifetime test of IrPt/Ti sample 1 by repeatedly scanning between 1.3 – 1.55 V, in 0.5 M KHSO<sub>4</sub> + 200 mM KCl. Rotation rate 1500 RPM, OER and CER currents gathered at a potential of 1.55 V.

Finally, we also probed the SiO<sub>x</sub> overlayer for stability over extended time duration, as this property is of vital importance when the electrodes are implemented for industrial purposes. The Ti-based anodes were developed for large-scale electrolysis, and they are designed for at least several years of stable continuous operation. As an accelerated stability test, a IrPt/Ti electrode was scanned repeatedly in and out of the mixed OER + CER region under rotation in 200 mM KCl. Catalyst stability in oxygen and chlorine electrocatalysis is usually the lowest under potentiodynamic conditions.<sup>82,300,301</sup> A total of one hundred cycles were applied over three intervals, amounting to roughly 75 minutes. The catalytic activity and CER selectivity were monitored over time (top and lower panel of Figure 7.9). Both the OER and CER activity increased slightly as the number of scans increased, but the CER selectivity stayed very close to a constant value of ~80%, suggesting that the overlayer integrity is well preserved. Transient

increases in activity (top panel of Figure 7.9) are perhaps due to changes in the interface between the overlayer and the catalyst. As mentioned in the discussion of Figure 7.7, the Si accumulated in the catalyst cracks could still be present in the form of its PDMS precursor, since it is not expected that the UV-ozone treatment is able to fully penetrate the cracks. During electrochemical measurements the precursor may yet still be converted into the oxide, altering the catalytic activity of the catalyst which is in close contact. It is possible that the cracked morphology in the catalyst surfaces is beneficial for the mechanical stability of the overlayer by providing ‘anchoring points’. All in all, the results in this section show that a  $\text{SiO}_x$  overlayer is capable of significantly increasing OER selectivity of an industrial-type catalyst. However, more research is needed to further improve this selectivity and reduce the negative impact on catalyst activity.

#### 7.4. Concluding remarks

The work described in this chapter shows that the concept of a  $\text{SiO}_x$ -based buried interface, which has been previously successful in preventing catalyst poisoning during hydrogen evolution on Pt, may also be a promising approach to enforcing selective oxygen evolution in acidic, chloride-containing electrolytes. Results of a  $\text{SiO}_x$  overlayer on Pt showed that this type of barrier is in principle capable of preventing chloride from reacting at the buried interface, while still allowing oxygen evolution to take place. The application of the same overlayer to Ir-based catalysts, which are much more representative of actual anodic materials in electrolyzers, led to varying success. On nanoparticulate, amorphous  $\text{IrO}_x$ , the  $\text{SiO}_x$  overlayers were not effective enough to lower the CER selectivity to satisfactory values. It is most likely that the  $\text{SiO}_x$  film integrity on this type of substrate was compromised, as the residual CER activity behaved kinetically very similar to that observed on unmodified  $\text{IrO}_x$  surfaces. The overlayer failure could be due to activity hotspots on the surface leading to intense gas evolution and delamination at the buried interface, or generally insufficient interaction of the overlayer with the catalyst. Application of an extra thick  $\text{SiO}_x$  overlayer to industrial-type mixed metal oxides led to a significant increase of OER selectivity, but also a notable activity drop. Some variation in the selectivity improvement was observed among different samples. This is likely due to the inhomogeneity of the different catalyst surfaces.

It must be stressed that the results presented here are preliminary, and that the  $\text{SiO}_x$  method can and should be further adjusted to be better suited to these specific surfaces. Mainly, the procedure for synthesizing the  $\text{SiO}_x$  overlayer, which in this chapter involved spin-coating, has not been optimized for samples with higher surface roughness. It must also be stressed that other oxide materials besides  $\text{SiO}_x$  could be employed as perm-selective overlayer, such as  $\text{MoO}_x$ ,  $\text{VO}_x$ , or (at high anodic polarization)  $\text{CeO}_x$ .<sup>281,302,303</sup> Alternatively, polymer modification or thin-membrane approaches might be used.<sup>165</sup> In any case, this study suggests that the morphology of the underlayer and its interaction with the overlayer are highly important in making the buried interface stable and effective. Further research into membrane-coated electrocatalysts may be a very promising pathway towards the realization of selective seawater electrolysis.

